www.rericjournal.ait.ac.th

New Method Coordinated Control of Battery Energy Storage Systems and Distributed Generations in Distribution Networks

Truong Ngoc-Hung*

ARTICLE INFO

Article history:
Received 30 December 2024
Received in revised form
06 March 2025
Accepted 24 March 2025

Keywords:
Battery energy storage system
Distributed generation
Microgrid
Solar power
Wind power

ABSTRACT

This paper studies on the microgrid operation modes based on a distribution network integrated with battery energy storage systems (BESSs) and distributed generations (DGs) such as solar and wind power plants. The location and capacity of DGs and BESSs are properly optimized to operate the distribution network. The IEEE 33-node distribution network integrated with solar power plants, wind power plants, and BESSs are modeled and simulated using the daily load and generation profiles. The mathematical modeling of the distribution network is applied to run power flow based on the practical load and generation profiles. For grid-following mode, the optimal location and capacity selection of the BESSs will improve the operation efficiency of the network. After integrating DGs and BESSs, the total active power loss is reduced by 27.6% and the voltage quality is also improved by 3.1%. Besides, the BESSs are capable to maintain the stability operation of the distribution network during a specified duration under a microgrid via the coordination between the BESSs and DGs after occurring a failure in the main grid. The simulation results have proven the capability of the BESSs to stabilize and improve the operation efficiency of the microgrid in both grid-following and grid-forming modes.

1. INTRODUCTION

Nowadays, renewable energy sources are gradually being exploited to replace traditional energy sources, however this trend has impacted on power system stability and reliability [1], [2]. The distribution networks are usually typical radial configurations in which power flow is followed one direction from generations to loads. When distributed generations are integrated into the power system, the power flow direction will be changed according to their operation modes. Therefore, the distribution network modeling integrated with renewable energy sources such as wind power, solar power, and energy storage systems needs to be conducted to carry out much research topics. In [3], a modeling method of distribution networks using the corrected Carson equations is proposed. Besides, the Newton - Raphson method is applied to solve the three-phase power flow of the distribution networks. The mathematical model for minimizing power losses in the distribution network reconfiguration has investigated to determine the bus voltage and branch current constraints [4], [5].

A microgrid is a standalone distribution network consisting of distributed generations and associated loads that uses local control to facilitate its connection and disconnection to/from with the main grid in order to maintain a standard service during disturbances without harming the integrity of the transmission grid [6]. In addition, the published works have comprehensively studied on control and management of microgrids [7], setting parameters to ensure microgrid stability [8], operation modes in real time taking into account the uncertainties of renewable energy sources [9], and reference frameworks to evaluate technical - environmental - economic aspects in microgrids [10]. Wind and solar power plants connected to the distribution networks have changed the power flow, therefore, maximizing the efficiency of these energy sources has been reviewed [11]-[18].

In microgrids, an energy storage system (*i.e.* the battery energy storage system - BESS) is used to stabilize and improve the operational efficiency through charging or discharging the BESS's energy and supplying to the distribution network [19]-[25]. In the BESS, the inverter makes it possible to control the BESS flexibly to generate or consume active and reactive power simultaneously. Therefore, the BESS can be operated to balance power, regulate voltage and it will be applied to replace gradually other traditional compensators. The authors in [19] analysed and evaluated the deeply penetration of renewable energies into distribution networks, leading to difficulties in maintaining permissible limits on power quality consisting of voltage and frequency variations. The paper proposed then the control method of energy storage system to regulate active and reactive power and improve power quality of the distribution network. The

*Department of I.T., FPT University- Quy Nhon AI Campus, Nhon Binh,, Quy Nhon, Binh Dinh, Vietnam.

[1]Corresponding author:
Email: hungtn19@fe.edu.vn

work [20] developed an approach for determining the BESS generation power based on the frequency and voltage control characteristics. In addition, many published works have studied the BESS control methods in microgrids such as the microgrid mathematical model [21], the active and reactive power controllers [22], the reverse droop control to stabilize microgrids [23], the optimization of the distribution network integrated with the BESS system [24]. The authors in [25] studied to determine the BESS capacity in order to maintain the distribution network voltage stability with large solar system integration.

From the aforementioned analysis, this paper focuses on establishing a mathematical modeling of a distribution network that integrates wind power plants, solar power plants, and battery energy storage systems based on mathematical models and real data. The operation modes of the distribution network are investigated to evaluate the operation efficiency of the network. In addition, the frequency and voltage control of the BESS are demonstrated in two operation modes consisting of the grid-following mode and the grid-forming mode to stabilize network when the main grid occurs a power outage or the renewable energy sources have a large disturbance. These operation modes are based on a real data such as a daily load profile, a local weather data which are applied to simulate the modified IEEE 33-node distribution network. From the simulation results, the paper proposes some recommendations for choosing the installed capacity of renewable energy sources and the battery energy storage systems according to the manufacturer's catalogue appropriately to improve the operational efficiency of the network. These findings can be applied to support the operational process of the practical distribution networks.

The new contributions of this paper can be summarized as follows: (i) Provide the mathematical modeling of wind power plants, solar power plants and battery energy storage systems connected to the distribution grid; (ii) Develop an algorithm flowchart to calculate the installed power capacity of wind power plants, solar power plants, and battery energy storage systems; (iii) Optimize the appropriate BESS capacity and location on the distribution network to improve the operation efficiency of the grid integrated with wind and solar power plants.

2. PROPOSED METHOD

2.1 Wind Power Plant Modeling

Wind turbines are divided into four main types including Double Fed Induction Generators (DFIGs) [15], [22] Spiral Case Induction Generators (SCIGs) [16], Wound Rotor Synchronous Generators (WRSGs) [17], and Permanent Magnet Synchronous Generators (PMSGs) [22]. According to [22], wind turbines consist of four basic techniques such as the fixed speed wind turbine (type 1 - fixed speed), the variable slip wind turbine (type 2 - variable slip), the dual power induction wind turbine (type 3 - DIFG), and the grid-connected wind turbine through full converter (type 4 - full converter).

While a DFIG wind turbine is operating, the mechanical power P_m and the stator power P_S are determined as follows:

$$P_m = T_m.\omega_r \quad (1)$$

$$P_s = T_{em}.\omega_s \quad (2)$$

where T_m is the mechanical torque on the rotor shaft, T_{em} is the electromagnetic torque, ω_s is the stator angular speed, ω_r is the rotor velocity.

The balance differential equation of the DFIG wind turbine is as follows:

$$J\frac{d\omega_r}{dt} = T_m - T_{em} \quad (3)$$

where J is the inertia constant

It is assumed that the rotor velocity is a constant, Equation (3) can be rewritten as follows:

$$J.\frac{d\omega_r}{dt} = 0 \quad (4)$$

It can be inferred the following equations:

$$T_m = T_{em} \quad (5)$$

$$P_m = P_s + P_r \quad (6)$$

$$P_r = P_m + P_s = -S.P_s \quad (7)$$

where,

$$s = \frac{\omega_s - \omega_r}{\omega_s}$$

The active and reactive power of the DFIG stator and rotor are determined as follows:

$$P_s = \frac{3}{2}(U_{ds}i_{ds} + U_{qs}i_{qs}) \quad (8)$$

$$Q_s = \frac{3}{2}(U_{qs}i_{ds} - U_{ds}i_{qs}) \quad (9)$$

$$P_r = \frac{3}{2}(U_{dr}i_{dr} + U_{qr}i_{qr}) \quad (10)$$

$$Q_r = \frac{3}{2}(U_{qr}i_{dr} - U_{dr}i_{qr}) \quad (11)$$

where P_s, Q_s are the stator active and reactive powers, respectively; P_r , Q_r are the rotor active and reactive powers, respectively; U_{qs}, U_{ds} are the stator voltages in the d-q reference frame; U_{qr}, U_{dr} are the rotor voltages in the d–q reference frame; i_{qs}, i_{ds} are the stator currents in the d-q reference frame; i_{qr}, i_{dr} are the rotor currents in the d-q reference frame.

In order to operate the DFIG as a generator according to two mentioned operation modes, both of the grid-side and rotor-side power converters must be able to control power flow in two directions. These two converters allow to the DFIG to operate in four P-Q complex plane quadrants, so it means that the DFIG is capable of generating reactive power to the grid. The reactive power exchange between the DFIG and the grid

can be independently controlled using these two converters [11].

2.2 Solar Photovoltaic System Modeling

Solar power is a green energy type from the sun that is converted into thermal or electrical energy. It has become popular in recent years due to its many benefits, including reducing greenhouse gas emissions, energy costs, and ensuring energy security. To generate electrical energy, solar power is exploited through solar photovoltaic systems. The advanced PV system control techniques such as the maximum power point tracking (MPPT), the model predictive current control (MPCC), and other inverter control techniques have applied to improving the PV system efficiency and flexibility [1], [2].

The equivalent circuit of a solar cell consists of an ideal current source in parallel with a reverse bias diode, both of which are connected to a load [1, 2]. In the circuit, the series resistor R_s and the shunt resistor R_p are parameters for characterizing the solar cell losses.

According to Kirchhoff's Current Law, the following equation is established:

$$I = I_{ph} - I_D - I_P \tag{12}$$

where I_{ph} is the current source which represents charge carrier generation in the semiconductor layer of the PV cell caused by incident radiation.

$$I_{ph} = [I_{SCr} + K_i(T - T_{ref})\frac{G}{1000} \tag{13}$$

where I_{SCr} is the short-circuit current, K_i is the short-circuit current coefficient according to the temperature, T and T_{ref} are the working temperature and the reference temperature (Kelvin degree), respectively, G is the solar irradiation on the surface of the cell (1000W/m2 is the nominal radiation).

I_p is the current flowing through the shunt resistor R_p, defined as:

$$I_P = \frac{V_D}{R_P} = \frac{V + R_S I}{R_P} \tag{14}$$

I_D is the current flowing through the diode, defined as:

$$I_D = I_0(e^{(\frac{qV_D}{AKT})} - 1) \tag{15}$$

where q is the electron charge constant ($q = 1.6.10^{-19}$C), K is the Boltzman constant ($K = 1.386503.10^{-23}$J/K), T is the battery temperature, Kelvin – K.

I_0 is the reverse saturation current of the reverse bias diode, defined as:

$$I_0 = I_{rs}\left[\frac{T}{T_{ref}}\right]^3 \exp\left[\left(q\frac{E_{g0}}{Ak}\right)\left(\frac{1}{T_{ref}} - \frac{1}{T}\right)\right] \tag{16}$$

I_{rs} is the saturation current of the reverse bias diode, defined as:

$$I_{rs} = \frac{I_{SCr}}{[\exp\left(\frac{qV_{0C}}{N_s kAT}\right) - 1]} \tag{17}$$

Combining Equations 12, 14, and 15 we get the characteristic equation as follows:

$$I = I_{ph} - I_0(e^{(\frac{qV_D}{AKT})} - 1) - \frac{V + R_S I}{R_P} \tag{18}$$

A is the ideal coefficient of solar cells. In the ideal case, $R_s \sim 0$ and $R_s \sim \infty$.

2.3 Battery Energy Storage System Modeling

A battery energy storage system (BESS) usually consists of three main components as illustrated in Figure 1 [20]-[22]. The battery cell arrays consist of multiple batteries connected in series and parallel. The power conversion system is a power electronic converter to convert the DC current to the AC current in the discharging mode or to inverter the AC current to the DC current in the charging mode. This system is based on the control signal of the control and monitoring system which is the core system of a BESS to control voltage, frequency and power at the point of common coupling.

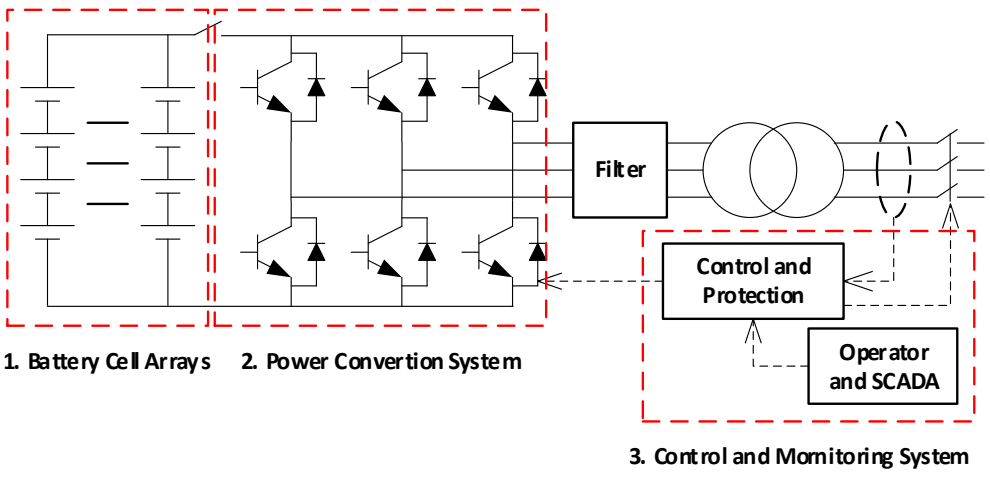

Fig. 1. Simplified block diagram of a BESS.

The State of Charge of a BESS must be satisfied the following equation:

$$SoC_{min} \leq SoC(t) \leq SoC_{max} \quad (19)$$

where SoC_{max} is the maximum State of Charge which is equivalent to the total rated capacity storage (C_n) and is proportional to the total number of cell arrays N_b, the number of cell arrays N_{bs} and the battery capacity C_b.

$$C_n = C_b(\frac{N_b}{N_{bs}}) \quad (20)$$

SoC_{min} is the minimum State of Charge.

$$SoC_{min} = (1 - DoD).SoC_{max} \quad (21)$$

where $DoD(\%)$ is the discharge capacity of the BESS.

The power converters can control a BESS to operate in four quadrants, therefore, the BESS can generate or consume active and reactive power independently [26].

2.4 Microgrid Modeling

Microgrids play a crucial role in modern energy management by enhancing resilience, efficiency, and sustainability in power systems. They integrate DGs such as solar panels, wind turbines, and battery energy storage systems, allowing for localized power generation and consumption. Besides, microgrids can address the renewable energy variability by incorporating energy storage systems (ESS), demand-side management, and intelligent forecasting to balance supply and demand. As defined in [6], a microgrid is a subsystem consisting of generators and consumers that utilizes local control to make its connection and disconnection to/from with the main distribution network in order to maintain a standard service quality during disturbances without harming. In addition, a microgrid consisting of distributed generations, micro turbines and especially energy storage systems can operate in the grid-following or grid-forming mode as shown in Figure 2. In the grid-forming mode, the microgrid enables self-control, protection, and management.

Observing the equivalent circuit as depicted in Figure 3, the microgrid consists of distributed generations (solar, wind power plants) and battery energy storage systems connected to the grid via voltage source converters, local loads modeled as RLC loads, and the microgrid is connected to the main grid through the RL filter, step-up transformer and the circuit breaker (CB). When the main grid appears a disturbance, the circuit breaker will open to operate the microgrid in the grid-forming mode. Therefore, the local loads are supplied power from the distributed generations and battery energy storage systems.

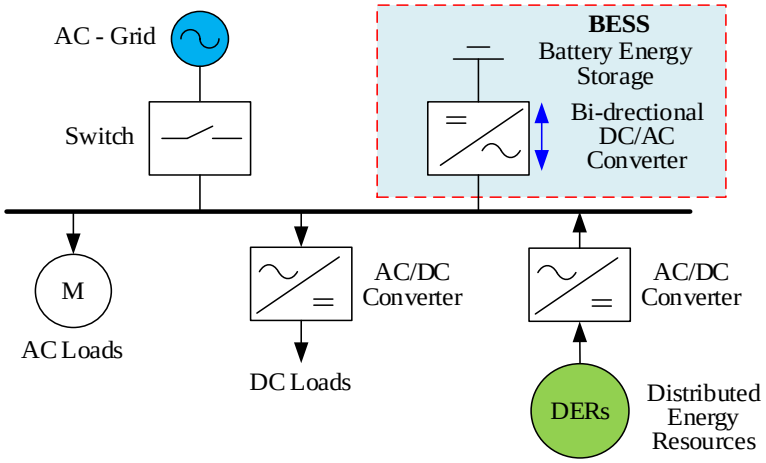

Fig. 2. Typical configuration of a microgrid.

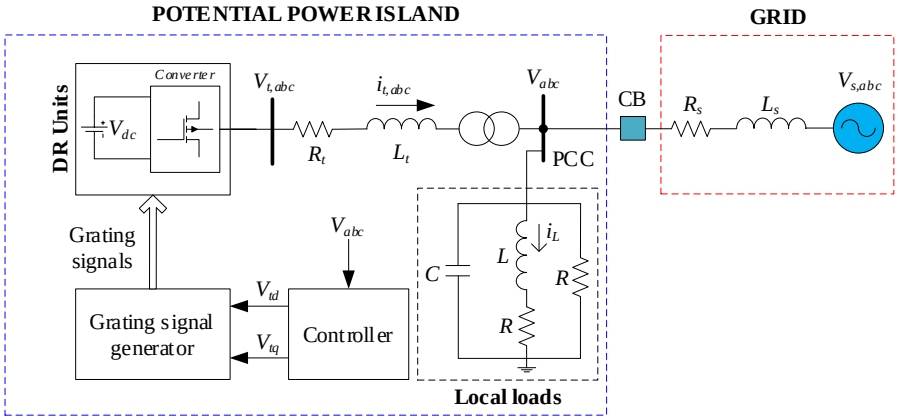

Fig. 3. Equivalent circuit of a microgrid model.

The microgrid model is represented by the following nonlinear equations:

$$\frac{di_{td}}{dt} = \omega i_{tq} - \frac{R_t}{L_t} i_{td} - \frac{v_d}{L_t} + \frac{v_{td}}{L_t} \quad (22)$$

$$\frac{dv_d}{dt} = \frac{1}{C} i_{td} - \frac{1}{RC} v_d - \frac{i_{Ld}}{C} \quad (23)$$

$$\frac{di_{Ld}}{dt} = \omega i_{Lq} + \frac{v_q}{L} - \frac{R_L}{L} i_{Ld} \quad (24)$$

$$\frac{di_{tq}}{dt} = -\omega i_{td} - \frac{R_t}{L_t} i_{tq} + \frac{v_{tq}}{L_t} \quad (25)$$

$$\frac{di_{Lq}}{dt} = -\omega i_{Ld} - \frac{R_L}{L} i_{Lq} \quad (26)$$

$$\omega C v_d = i_{tq} - i_{Lq} \quad (27)$$

Analytically, linearization of the above nonlinear equations uses the first-order Taylor series expansion about the operative point, the state space matrix is obtained as follows:

$$A = \begin{bmatrix} -\frac{R_t}{L_t} & \omega_0 & 0 & -\frac{1}{L_t} \\ \omega_0 & -\frac{R_L}{L} & -2\omega_0 & \frac{R_L C \omega_0}{L} - \frac{\omega_0}{R} \\ 0 & \omega_0 & -\frac{R_L}{L} & \frac{1}{L} - \omega_0^2 C \\ \frac{1}{C} & 0 & -\frac{1}{C} & -\frac{1}{RC} \end{bmatrix} \quad (28)$$

$$B^T = \begin{bmatrix} \frac{1}{L_T} & 0 & 0 & 0 \end{bmatrix} \quad (29)$$

$$C = [0 \quad 0 \quad 0 \quad 1] \quad (30)$$

$$X^T = [i_{td} \quad i_{tq} \quad i_{Ld} \quad v_d] \quad (31)$$

2.5 Power Flow Method

Distribution networks are a part of a power system consisting of lines and substations with a voltage level up to 110 kV. Distribution networks are to transmit power from intermediate substations to electrical loads and they mostly have a radial structure, having many different load types [3], [4], [27]. In addition, the distribution networks are becoming active systems with the integration of distributed generations (wind power plants, solar power plants, micro turbines) and battery energy storage systems which are usually connected to the networks via power converters.

In this paper, the power flow optimization formulation is described in Figure 4 for minimizing the power losses in the distribution network as presented by Equation (32) while it must be completely satisfied the constraints consisting of the active and reactive power balance by Equations (33), (34), the bus voltage limitations by Equation (35), and the branch current limitations by Equation (36).

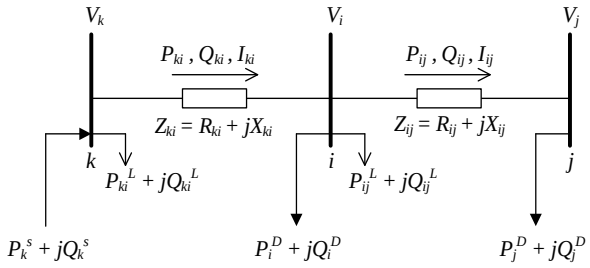

Fig. 4. Simplified distribution network model.

The objective function is as follows:

$$\text{Min } P_{Loss} = \sum_{ij \in m} P_{ij}^L \quad (32)$$

The active and reactive power balance constraints are as follows:

$$P_i^S + \sum_{k=1}^{n} P_{ki} = \sum_{j=1}^{n} P_{ij} + \sum_{j=1}^{n} P_{ij}^L + P_i^D \quad (33)$$

$$Q_i^S + \sum_{k=1}^{n} Q_{ki} = \sum_{j=1}^{n} Q_{ij} + \sum_{j=1}^{n} Q_{ij}^L + Q_i^D \quad (34)$$

The bus voltage constraints are as follows:

$$V_{min} \le |V_i| \le V_{max} \quad (35)$$

The branch current constraints are as follows:

$$|I_{ij}| \le I_{ij}^{max} \quad (36)$$

where m is the number of branches; n is the number of buses; P_{ij}^L, Q_{ij}^L are the active and reactive power losses; respectively; P_{ij}, Q_{ij} are the active and reactive power of the branch ij, respectively. P_i^S, Q_i^S are the active and reactive power injection at the bus i, respectively. V_{min}, V_{max} are the minimum and maximum voltage magnitudes at the bus i, respectively. $|V_i|$ is the load voltage magnitude of the bus i. Q_i^D is the reactive load power of the bus i. $|I_{ij}|$, I_{ij}^{max} are the current amplitude and maximum current of the branch ij, respectively. R_{ij}, X_{ij} are the resistance and reactance of the branch ij, respectively.

3. SIMULATION RESULTS AND DISCUSSION

3.1 Test System Description

This paper uses the IEEE 33-node distribution network to apply the proposed method [28]. The methodology for simulating and analyzing the IEEE 33-node distribution network involves several key steps, including data collection, model calibration, and simulation. Some assumptions for this network include: the network operates under balanced, steady-state conditions; line impedances and loads are assumed to be constant for the duration of the simulation. This is a radial distribution network, including a main branch from Node 1 to Node 18 and three sub-branches at Nodes 2, 3, and 6. The total load power is $P = 3655$ kW and $Q = 2260$ kVAr. The

line and transformer data of the IEEE 33-node network is cited in [29]. To simulate the proposed method, the DGs are assumed that they are connected at all nodes of the network, then power flow is calculated to determine the optimal location, power loss and installed power of the DGs while the constraints of power balance, voltage and current limitations on the branches are within the acceptable limits. In addition, the battery energy storage system is considered as the "heart" of the distribution network and microgrid when the microgrid is integrated to renewable energy sources (wind and solar power plants). The BESS plays a vital role to maintain power balance (P,Q) and microgrid voltage stability as the renewable energy sources and the main grid have a fluctuation or disturbance. The reference [30] addressed the role of BESS to maintain within the microgrid under changing conditions and proposed the comprehensive method to optimize the power distribution between photovoltaic system, BESS, and the grid. In addition, this paper also studies and evaluates the microgrid islanded mode in which it acts as an independent microgrid for a 3-hour duration when the main grid and the distributed generations have an outage for supplying electricity to the network. Based on each scenario, the paper proposes the procedure to calculate correctly the BESS' capacity, thereby improving the operational efficiency of the microgrid. To perform numerical simulations using the PSS/Adept software, the IEEE 33-node distribution network without distributed generations has up to 18 nodes with more than 5% voltage drop, which are located at the ends of the radial branches. In order to improve the voltage quality of the distribution network, the paper proposes operation scenarios with the integration of distributed generations and battery energy storage systems to overcome voltage drop, reduce power loss and improve stability. The power flow calculation of the distribution network is carried out for all case studies to determine the operation parameters such as the bus voltage magnitudes, the branch currents, and the line power losses, *etc.* to evaluate power quality before and after integrating with the distributed generations and the battery energy storage system.

3.2 Scenario 1: Grid-Following Mode

The load profile of the IEEE 33-node distribution network is presented in Figure 5, in which the main grid is the 110/13.8 kV transformer, the distributed generations and the battery energy storage system will be installed to supply power to local loads. The distributed generation locations and capacities are optimized to minimize the power loss; however the constraints consisting of the power balance, the limitations of bus voltage and branch current must be satisfied. According to the IEEE 33-node distribution network data, the maximum total active and reactive load powers are $P_{max} = 3655$ kW and $Q_{max} = 2260$ kVAr, respectively. It can be obviously seen from this profile that the peak load power is at the time 16:30.

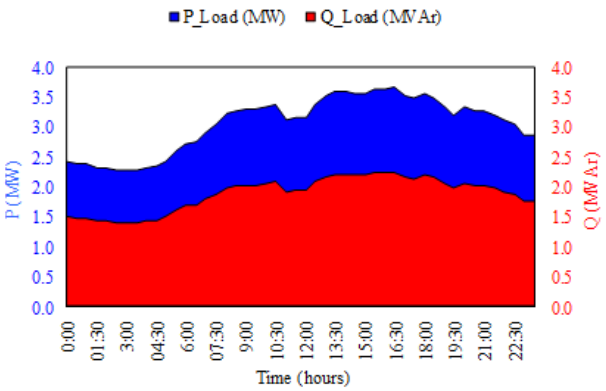

Fig. 5. Load profile.

The load profile is taken from the real data and is assumed to be proportional to the IEEE 33-node distribution network in a 24-hour daily duration. This graph is drawn from 48 points equivalent to 30 minutes per sample. To determine the parameters of distributed generations, this paper uses the real data on April 1, 2024 in the authors' country. For solar power plants, the solar irradiance data have an operation time from 06:00 to 18:00, and the solar power peak is 0.76 kW at the time of 11:45. For wind power plants, the wind speed is also collected from 00:00 to 23:30. From the simulation results, the optimal location to place the distributed generations and the battery energy storage system is the node 6 because the active power loss of this case is the smallest one among the simulated cases in this paper as shown in Figure 6.

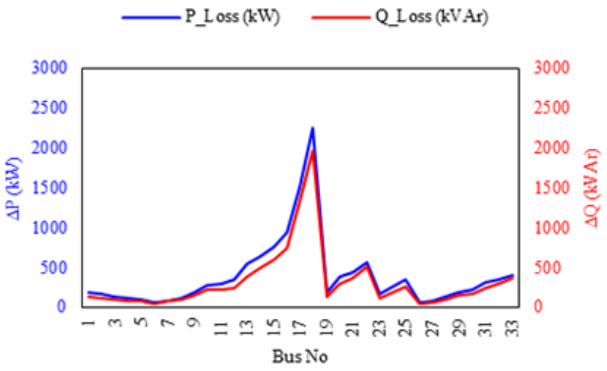

Fig. 6. Active and reactive power losses when DGs are installed at each node.

For the scenario 1, the IEEE 33-node distribution network will still be connected to the main power supply at the node 1 which acts as a swing bus. The distributed generations are installed at the node 6, acting as a voltage control node, with the generation power of the optimal power calculated in the above steps. In order to meet the load demand of the whole network within 24 hours (with 48 samples of data collection), this paper changes the load capacity at the nodes and runs the power flow formulation for all cases to determine the optimal generation powers of the solar and wind power plants at the node 6 as shown in Figure 7.

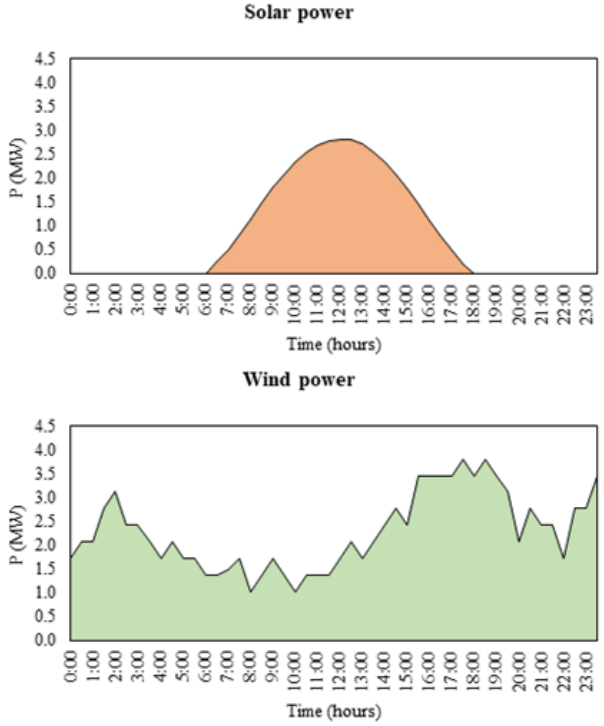

Fig. 7. Solar and wind power profiles.

To operate the network according to the 24-hour load profile, the 2.8MW solar power plant, the 3.82MW wind power plant, and the 2.5MVA battery energy storage system are determined for the scenario 1. For this scenario, the battery energy storage system plays an important role to maintain a stable system by charging or discharging when the distributed generation power varies due to weather and climate conditions. In addition, the battery energy storage system will continuously operate at the State of Charge between 20% and 100% corresponding to the charging and discharging limits of the battery to balance the power between the generation power and the load power as well as to stabilize the distribution network voltage and frequency. The battery energy storage system will be charged when the total distributed generation power is greater than the total load power and will be discharged to generate power to the distribution network for compensating the lack of generation power.

In the scenario 1, the distributed generations mainly generate active power to the distribution network because the power supply source at the node 1 plays as a swing node, so the distributed generations only meet the active power balance condition and ensure the node voltage (13.8 kV). The reactive power to supply for the loads in this scenario is still received from the transmission grid for the node 1. This paper focuses on calculating and optimizing the active power for each distributed generation, the reactive power will be supplemented and met from the transmission grid. The capacity of the battery energy storage system is also calculated and selected for charging and discharging to meet the load demand along with the solar and wind power sources. The power flow results of the scenario 1 are shown in Figure 8.

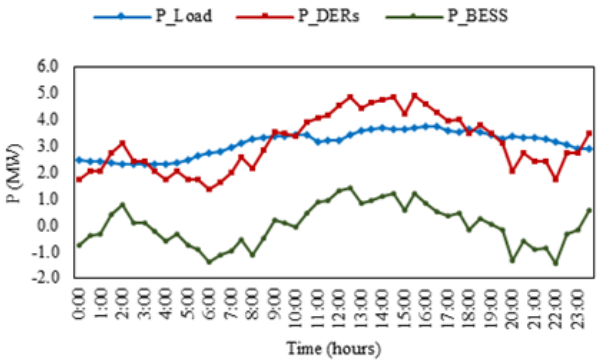

Fig. 8. IEEE 33-node grid load and generation profiles.

3.3 Scenario 2: Grid-Forming Mode

In this scenario, when the main grid appears a fault, the upstream circuit breaker will cut off and the IEEE 33-node distribution network can be independently operated as a microgrid (islanded mode). The distributed generations and the battery energy storage system on the microgrid will be calculated and distributed to operate the microgrid normally until the main grid is restored. In the grid-forming mode, the IEEE 33-node distribution network is operated as a microgrid (islanded model mode), the battery energy storage systems and the distributed generations will generate active and reactive power to balance the power between generations and loads as well as to meet the voltage and current stability conditions to operate the microgrid normally. Thus, the operation problem needs to be solved differently from the scenario 1 which is to generate reactive power of the distributed generations and the battery energy storage systems.

In this case, when the IEEE 33-node distribution network becomes a microgrid, the generation active and reactive power and total power loss are reduced compared to the scenario 1. However, the capacity of the battery energy storage system and the distributed generations must be greater in the scenario 1 to provide reactive power for the loads. The simulation results of the scenario 2 show that the battery energy storage system can maintain the normal operation of the microgrid within 3 hours after the main grid occurs a fault by tripping the upstream circuit breaker. The generation power calculation of the distributed generations will ensure the power factor in the continuous and long-term operation mode of 0.85. It is assumed that the loss of the battery energy storage system components (*e.g.* inverters, batteries, *etc.*) is negligible. Thus, the generation power of the battery energy storage system will be calculated to ensure that the microgrid operates in both of operation conditions including: The first mode is to generate or consume the active and reactive power as shown in Figure 9; the second one is to maintain the microgrid within 3 hours by generating the active and reactive power in case of the main grid failure.

In the scenario 2, it is assumed that all the distributed generations do not operate for the worst case, and the loads work at the maximum power (at the time 16:30) with the active and reactive power $P_{Gen} =$ 3.72 MW and $Q_{Gen} =$ 2.311 MVAr ($S =$ 4.4 MVA). To supply the above power (the total load power $S =$

4.4 MVA and the battery energy storage system capacity 11.16 MWh), this paper chooses two units of battery energy storage systems, having the total capacity of $S_{total} = 4.5$ MVA and $E_{pin} = 14.664$ MWh with SoC from 20% to 100%. The 2500kVA unit will be connected to the distribution network to operate the network continuously in the scenario 1, and the 2000kVA unit will be controlled by the EMS system to connect to the microgrid when it is operated in the grid-forming mode (in the scenario 2). As a result, the capacity of distributed generations and the battery energy storage systems will be as follows: the solar power plant of 3.3 MVA (pf = 0.85), the wind power plant of 4.5 MVA (pf = 0.85), and the battery energy storage system of 4.5 MVA (2 units).

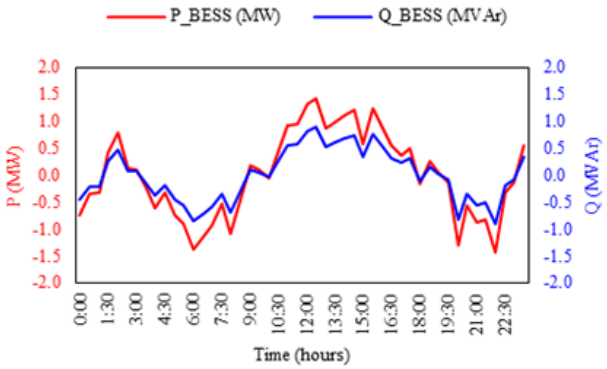

Fig. 9. Active and reactive power of the BESS.

4. CONCLUSION

This paper has studied operating scenarios corresponding to the actual load profiles, thereby the capacities of the distributed generations and battery energy storage systems are correctly determined to operate the distribution network in the stability and reliability status. Two operation scenarios consisting of the grid-following and grid-forming modes are comprehensively investigated in this paper. For the grid-following mode, the distributed generations and the battery energy storage systems are placed at the node 6, the voltage quality has been improved. The lowest voltage magnitude on the distribution network without distributed generations and battery energy storage system is at the node 33 of 0.921 pu equivalent to 7.9%. On the other hand, after integrating the distributed generations and the battery energy storage systems into the network, the voltage magnitude of the node 33 is 0.969 pu equivalent to 3.1%. Besides, the total power loss was also significantly reduced. Before the distributed generations are integrated into the network, the power loss is $P_{loss} = 192.208$ kW and $Q_{loss} = 128.376$ kVAr. However, the power loss is $P_{loss} = 89.735$ kW and $Q_{loss} = 65.637$ kVAr after the distributed generations are integrated into the network. For the grid-forming mode, the battery energy storage system can maintain the normal operation of the microgrid within 3 hours after the main grid occurs a fault by tripping the upstream circuit breaker. Additionally, the total power loss is $P_{loss} = 65$ kW and $Q_{loss} = 50.8$ kVAr. From the simulation results, some key findings can be summarized in this paper as follows: Formulate the mathematical models for wind power plants, solar power plants, and battery energy storage systems connected to the distribution network; Design an algorithm flowchart to determine the installed power capacity of wind and solar power plants, as well as battery energy storage systems; Optimize the capacity and placement of battery energy storage systems within the distribution networks to enhance the operational efficiency of the network integrated with wind and solar energy sources.

The next research direction on sensitivity analysis of parameters for power grids integrated with BESS will focus on evaluating the impact of key parameters such as BESS capacity, charging/discharging power, control strategies, and installation location within the grid. Additionally, the research will expand to real-time sensitivity analysis to optimize BESS operation under fluctuating load conditions and variable renewable energy sources. Machine learning methods can also be applied to enhance the analytical models, improving the accuracy and efficiency of the system.

REFERENCES

[1] Yatimi H. and E.H. Aroudam. 2015. A detailed study and modeling of photovoltaic module under real climatic conditions. *International Journal of Electronics Electrical Engineering* 3(3): 171-176.

[2] Boucenna K., Sebbagh T., and Benchouia N.E., 2023. Modeling, optimization, and techno-economic assessment of a hybrid system composed of photovoltaic-wind-fuel cell and battery bank. *Journal Européen des Systèmes Automatisés* 56(1): 29.

[3] Ayanlade S.O., Jimoh A., Ogunwole E.I., Jimoh A.B., and Ezekiel S.O., 2023. Mathematical modelling of the distribution network for three-phase power flow analysis. In *Proceedings of the 11th International Conference on Mathematical Modeling In Physical Sciences.* Belgrade, Serbia, 5-8 September.

[4] Mahdavi M., Alhelou H.H., Hatziargyriou N.D., and Al-Hinai A., 2021. An efficient mathematical model for distribution system reconfiguration using AMPL. *IEEE Access* 9:79961-79993.

[5] Belhadjer Y., Ait Abbas H., Laroussi K., Bousbaine A., Fergani O., and Mazari A., 2024. Optimizing DC microgrid systems for efficient electric vehicle battery charging in Ain El Ibel, Algeria. *International Journal of Engineering* 37(10): 1891-1900.

[6] Mahmoud M.S., Hussain S.A., and Abido M.A., 2014. Modeling and control of microgrid: An overview. *Journal of the Franklin Institute* 351(5): 2822-2859.

[7] Moradian M., Tabatabaei F.M., and Moradian S., 2013. Modeling, control and fault management of microgrids. *Smart Grid and Renewable Energy* 4(1): 99-112.

[8] Ma Q., Wei W., Chen X., and Mei S., 2022. The admissible set of parameters guaranteeing

small-signal stability of a microgrid. *IET Renewable Power Generation* 16(13): 2721-2731.

[9] Bui V.-H., Song N.-O., Lee J.-H., and Kim H.-M., 2015. Mathematical modeling of real-time scheduling for microgrid considering uncertainties of renewable energy sources. *International Journal of Smart Home* 9(7): 271-284.

[10] El Sayed A., Poyrazoglu G., and Ahmed E.E., 2024. An integrated framework for techno-enviro-economic assessment in nanogrids. *International Journal of Renewable Energy Development* 13(2): 340-350.

[11] Lei Y., Mullane A., Lightbody G., and Yacamini R., 2006. Modeling of the wind turbine with a doubly fed induction generator for grid integration studies. *IEEE Transactions on Energy Conversion* 21(1): 257-264.

[12] Chaudhuri A., Datta R., Kumar M.P., Davim J.P., and Pramanik S., 2002. Energy conversion strategies for wind energy system: Electrical, mechanical and material aspects. *Materials* 15(3): 1232.

[13] Singh M. and S. Santoso. 2011. Dynamic models for wind turbines and wind power plants. National Renewable Energy Lab.(NREL), Golden, CO (United States).

[14] Chong C., Rigit A., and Ali I., 2021. Wind turbine modelling and simulation using Matlab/SIMULINK. In *Proceedings of the 13th International UNIMAS Engineering Conference 2020 (ENCON 2020)*, Kuching, Malaysia, 27-28 October. IOP Publishing.

[15] Muller S., Deicke M., and De Doncker R.W., 2002. Doubly fed induction generator systems for wind turbines. *IEEE Industry applications magazine* 8(3): 26-33.

[16] Garcia D. and J. Luis. 2009. Modeling and control of squirrel cage induction generator with full power converter applied to windmills, University of OULU.

[17] Kwon D.Y., Bang T.K., Kim C.W., Shin K.H., and Choi J.Y., 2020. Experimental verification and electromagnetic characteristics analysis of wound-rotor synchronous generator using magnetic equivalent circuit method. *AIP Advances* 10(1): 015014.

[18] Ahmadigorji M. and M. Mehrasa. 2023. A robust renewable energy source-oriented strategy for smart charging of plug-in electric vehicles considering diverse uncertainty resources. *International Journal of Engineering* 36(4): 709-719.

[19] Shin S.S., Oh J.S., Jang S.H., Cha J.H., and Kim J.E., 2017. Active and reactive power control of ESS in distribution system for improvement of power smoothing control. *Journal of Electrical Engineering Technology* 12(3): 1007-1015.

[20] Akagi S., Yoshizawa S., Yoshinaga J., Ito M., Fujimoto Y., Hayashi Y., Yano T., Nakahata H., Hisada T., and Tran X.M., 2016. Capacity determination of a battery energy storage system based on the control performance of load leveling and voltage control. *Journal of International Council on Electrical Engineering* 6(1): 94-101.

[21] Zulkifly Z., Yusoff S.H., Tumeran N.L., and Razali N.S.I., 2023. Battery energy storage system (BESS) modeling for microgrid. *IIUM Engineering Journal* 24(1): 57-74.

[22] Gao J.T., Shih C.H., Lee C.W., and Lo K.Y., 2022. An active and reactive power controller for battery energy storage system in microgrids. *IEEE Access* 10: 10490-10499.

[23] Akdogan M.E. and S. Ahmed. 2021. Energy storage system (ess) for compensating unbalanced multi-microgrids using modified reverse droop control. In *Proceedings of 2021 IEEE Applied Power Electronics Conference and Exposition (APEC)*, Phoenix, AZ, USA, 14-17 June: IEEE.

[24] Eyisi C., Al-Sumaiti A.S., Turitsyn K., and Li Q., 2019. Mathematical models for optimization of grid-integrated energy storage systems: a review. In *Proceedings of 2019 North American Power Symposium (NAPS)*, Wichita, KS, USA, 13-15 October: IEEE.

[25] Mansour O.M.A.A., 2016. Determining the power and energy capacity of a battery energy storage system utilizing a smoothing feeder profile to accommodate high photovoltaic penetration on a distribution feeder. *MS Thesis*, Portland State University, US.

[26] Biroon R.A., Pisu P., and Schoenwald D., 2020. Inter-area oscillation damping via hybrid LQR state feedback control of large-scale battery. In *2020 52nd North American Power Symposium (NAPS)*, 2021, pp. 1-6: IEEE.

[27] Foomani A.H., Moradlou M., and Nazarian P., 2024. Utilizing a new voltage stability index in distribution power system in presence of wind turbine units. *International Journal of Engineering* 37(4): 711-724.

[28] Dharageshwari K. and C. Nayanatara. 2015. Multiobjective optimal placement of multiple distributed generations in IEEE 33 bus radial system using simulated annealing. In *Proceedings of 2015 International Conference on Circuits, Power and Computing Technologies*. Nagercoil, India, 19-20 March: IEEE.

[29] Almabsout E.A., El-Sehiemy R.A., An O.N.U., and Bayat O., 2020. A hybrid local search-genetic algorithm for simultaneous placement of DG units and shunt capacitors in radial distribution systems. *IEEE Access* 8: 54465-54481.

[30] Reguieg Z., Bouyakoub I., and Mehedi F., 2025. Integrated optimization of power quality and energy management in a photovoltaic-battery microgrid. *Renewable Energy* 241: 122358.